The Global Atmospheric Circulation on Moist Isentropes

Olivier Pauluis, *et al.*

Science **321**, 1075 (2008);
DOI: 10.1126/science.1159649

References and Notes

1. N. S. Lewis, D. G. Nocera, *Proc. Natl. Acad. Sci. U.S.A.* **103**, 15729 (2006).
2. N. Nelson, A. Ben-Shem, *Nat. Rev. Mol. Cell Biol.* **5**, 971 (2004).
3. J. Barber, *Philos. Trans. R. Soc. London Ser. A* **365**, 1007 (2007).
4. A. J. Bard, M. A. Fox, *Acc. Chem. Res.* **28**, 141 (1995).
5. T. A. Betley, Q. Wu, T. Van Voorhis, D. G. Nocera, *Inorg. Chem.* **47**, 1849 (2008).
6. R. I. Cukier, D. G. Nocera, *Annu. Rev. Phys. Chem.* **49**, 337 (1998).
7. M. H. V. Huynh, T. J. Meyer, *Chem. Rev.* **107**, 5004 (2007).
8. R. Eisenberg, H. B. Gray, *Inorg. Chem.* **47**, 1697 (2008).
9. K. N. Ferreira, T. M. Iverson, K. Maghlaoui, J. Barber, S. Iwata, *Science* **303**, 1831 (2004), published online 5 February 2004; 10.1126/science.1093087.
10. S. Iwata, J. Barber, *Curr. Opin. Struct. Biol.* **14**, 447 (2004).
11. J. Yano *et al.*, *Science* **314**, 821 (2006).
12. B. Loll, J. Kern, W. Saenger, A. Zouni, J. Biesiadka, *Nature* **438**, 1040 (2005).
13. S. Trassati, in *Electrochemistry of Novel Materials*, J. Lipkowski, P. N. Ross, Eds. (VCH, New York, 1994), chap. 5.
14. J. O. Bockris, T. J. Otagawa, *J. Electrochem. Soc.* **131**, 290 (1984).
15. M. R. Tarasevich, B. N. Efremov, in *Electrodes of Conductive Metal Oxides*, S. Trasatti, Ed. (Elsevier, Amsterdam, 1980), chap. 5.
16. M. Yagi, E. Tomita, S. Sakita, T. Kuwabara, K. Nagai, *J. Phys. Chem. B* **109**, 21489 (2005).
17. V. Y. Shafirovich, N. K. Khannanov, V. V. Strelets, *Nouv. J. Chim.* **4**, 81 (1980).
18. B. S. Brunschwig, M. H. Chou, C. Creutz, P. Ghosh, N. Sutin, *J. Am. Chem. Soc.* **105**, 4832 (1983).
19. Materials and methods, videos of an active electrode, and figs. S1 to S4 are available as supporting material on *Science* Online.
20. In a typical experiment, >40 C are passed over 8 hours, whereas oxidation of all the Co^{2+} in solution requires 1.9 C per oxidation-state change.
21. K. D. Bomben, J. F. Moulder, P. E. Sobol, W. F. Stickel, in *Handbook of X-Ray Photoelectron Spectra: A Reference Book of Standard Spectra for Identification*, J. Chastain, Ed. (Perkin Elmer, Eden Prairie, MN, 1992).
22. T. Irebo, S. Y. Reece, M. Sjödin, D. G. Nocera, L. Hammarström, *J. Am. Chem. Soc.* **129**, 15462 (2007).
23. C. J. Chang, Z.-H. Loh, C. Shi, F. C. Anson, D. G. Nocera, *J. Am. Chem. Soc.* **126**, 10013 (2004).
24. W. H. Casey, *J. Colloid Interface Sci.* **146**, 586 (1991).

25. This work was supported by a grant from the NSF Chemical Bonding Center (CHE-0802907). M.W.K. is supported by a Ruth L. Kirchenstein National Research Service Award postdoctoral fellowship provided by NIH (F32GM07782903). We thank E. Shaw for obtaining XPS spectra, G. Henoch for providing the videos in the supporting online material, and Y. Surendranath for many productive discussions.

Supporting Online Material

www.sciencemag.org/cgi/content/full/1162018/DC1
Materials and Methods
Figs. S1 to S4
Movies S1 and S2

19 June 2008; accepted 18 July 2008
Published online 31 July 2008;
10.1126/science.1162018
Include this information when citing this paper.

The Global Atmospheric Circulation on Moist Isentropes

Olivier Pauluis,[1]* Arnaud Czaja,[2] Robert Korty[3]

The global atmospheric circulation transports energy from the equatorial regions to higher latitudes through a poleward flow of high-energy and -entropy parcels and an equatorward flow of air with lower energy and entropy content. Because of its turbulent nature, this circulation can only be described in some averaged sense. Here, we show that the total mass transport by the circulation is twice as large when averaged on moist isentropes than when averaged on dry isentropes. The additional mass transport on moist isentropes corresponds to a poleward flow of warm moist air near Earth's surface that rises into the upper troposphere within mid-latitudes and accounts for up to half of the air in the upper troposphere in polar regions.

Earth absorbs shortwave radiation from the Sun and emits back longwave radiation to space. Although the total amounts of energy received and emitted are about equal, Earth absorbs more energy than it emits in the equatorial regions and emits more energy than it absorbs at high latitudes (*1*). Such imbalance requires an energy transport by the atmosphere and the oceans, with the former responsible for the bulk of the transport in mid-latitudes (*2*). Determining the relationship between the atmospheric energy transport and the global distribution of temperature and humidity is a central question for our understanding of the Earth's climate.

Averaging the global atmospheric circulation usually implies computing a zonal and temporal mean over a sufficiently long period. One of the most common descriptions is the Eulerian mean circulation (*1*), obtained by averaging the flow at constant pressure or geopotential height. The Eulerian mean stream function Ψ_p is defined as

$$\Psi_p(p,\phi) = \frac{1}{\tau}\int_0^\tau \int_0^{2\pi} \int_p^{p_{\mathrm{surf}}} va\cos\phi \frac{dp}{g} d\lambda dt \qquad (1)$$

Here, p is pressure, ϕ is latitude, τ is the time period over which the average is computed, p_{surf} is surface pressure, λ is longitude, a is Earth's radius, v is the meridional velocity, and g is the gravitational acceleration. Figure 1A shows the annual mean stream function on pressure surfaces based on the National Centers for Environmental Prediction–National Center for Atmospheric Research (NCEP-NCAR) Reanalysis monthly data (*3*) from January 1970 to December 2004. The Eulerian-mean circulation exhibits a three-cell structure in each hemisphere: the Hadley cell in the tropics, the Ferrel cell in mid-latitudes, and a polar cell at high latitudes. The Hadley and polar cells, with air parcels moving poleward at high altitude and equatorward at low altitude, are direct circulations that transport energy toward the poles. In the Ferrel cell, the flow is poleward near the surface and equatorward at high altitude. This corresponds to an energy transport toward the equator. Nonetheless, in mid-latitudes, synoptic-scale (~1000 km) eddies transport more energy toward the poles than is brought equatorward by the Ferrel cell, so that the total energy transport in the atmosphere remains poleward.

An alternative to the Eulerian mean circulation is to average the circulation on isentropic surfaces (*4*–*6*). In atmospheric sciences, it is common to use the potential temperature θ instead of entropy. The potential temperature is given by $\theta = \left(\frac{p_0}{p}\right)^{\frac{R}{C_p}} T$, with p the pressure, R the ideal gas constant, C_p the specific heat, T the temperature, and p_0 = 1000 mbar an arbitrary reference pressure. Potential temperature is conserved for reversible adiabatic transformations in the absence of a phase transition, and a surface of constant potential temperature corresponds to isentropic surfaces. The stream function $\Psi_\theta(\theta,\phi)$ on potential temperature surfaces is defined by

$$\Psi_\theta(\theta_0,\phi) = \frac{1}{\tau}\int_0^\tau \int_0^{2\pi} \int_0^{p_{\mathrm{surf}}} H(\theta_0-\theta) va\cos\phi \frac{dp}{g} d\lambda dt \qquad (2)$$

Here, $H(x)$ is the Heavyside function, with $H(x) = 1$ for $x \geq 0$ and $H(x) = 0$ for $x < 0$. Figure 1B shows the annual mean stream function on potential temperature surfaces based on the NCEP-NCAR Reanalysis daily data from January 1970 to December 2004.

In contrast to the Eulerian mean circulation, the circulation in isentropic coordinates exhibits a single overturning cell in each hemisphere. Because the atmosphere is stratified in potential temperature ($\partial_z\theta > 0$), the isentropic circulation corresponds to a poleward flow at upper levels balanced by a return flow near Earth's surface—in the direction opposite to the Eulerian mean circulation (*4*). The meridional mass transport on an isentrope can be written as

$$\overline{\rho_\theta v} = \overline{\rho}_\theta \overline{v} + \overline{\rho_\theta' v'} \qquad (3)$$

[1]Courant Institute of Mathematical Sciences, New York University, 251 Mercer Street, New York, NY 10012, USA. [2]Space and Atmospheric Physics Group, Department of Physics, Imperial College, Huxley Building, Room 726, London SW7 2AZ, UK. [3]Department of Atmospheric Sciences, Texas A&M University, 3150 TAMU, College Station, TX 77843–3150, USA.

*To whom correspondence should be addressed. E-mail: pauluis@cims.nyu.edu

where $\rho_\theta = -g^{-1}\frac{\partial p}{\partial \theta}$ is the isentropic density, the overline indicates a time and zonal average, and the prime a departure from such a temporal and zonal average (i.e., $f' = f - \overline{f}$). The first term on the right-hand side is the mass transport by the zonal and time mean circulation and is in the same direction as the Eulerian mean circulation. The second term is the mass transport by the eddies and dominates the isentropic mass transport in mid-latitudes. This eddy mass transport is similar to the Stoke's drift in shallow water waves (*7*). The circulation on isentropic surfaces is similar to the transformed Eulerian mean circulation in which a residual circulation is computed by accounting for the eddy mass transport (*8*–*10*). Because the potential temperature of an air parcel is approximately conserved in the free troposphere in the absence of condensation, the isentropic circulation is more indicative of the parcel trajectories than the circulation obtained through Eulerian averaging.

A key issue when discussing the isentropic circulation lies in that the entropy of moist air is not uniquely defined (*11*). Indeed, the specific entropy of water vapor can be specified only to within an additive constant. As a consequence, the entropy of moist air can be known only up to this constant multiplied by the water concentration. To test whether this has an impact on the averaged circulation, we computed the circulation by using the equivalent potential temperature, θ_e, to define isentropic surfaces (*11*). The equivalent potential temperature is conserved for reversible adiabatic transformations, including phase transitions. In contrast to the potential temperature, it includes a contribution from the latent heat content of water vapor and can be roughly approximated by $\theta_e \sim \theta + \frac{L_v}{C_p} q$, with L_v the latent heat of vaporization and q the water vapor concentration. Both θ and θ_e define two distinct sets of isentropic surfaces, and correspond to a correct definition of the thermodynamic entropy. We refer here loosely to "dry" isentropes as surfaces of constant potential temperature and to "moist" isentropes as surfaces of constant equivalent potential temperature. The stream function on moist isentropes, $\Psi_{\theta_e}(\theta_e, \phi)$, is defined by

$$\Psi_{\theta_e}(\theta_{e0}, \phi) = \frac{1}{\tau}\int_0^{\tau}\int_0^{2\pi}\int_0^{p_{surf}} H(\theta_{e0} - \theta_e) va\cos\phi \frac{dp}{g} d\lambda dt \quad (4)$$

Figure 1, B and C, compares the stream functions on dry and moist isentropes. Although qualitatively similar, the two circulations differ substantially in that the total mass transport on moist isentropes is approximately twice that on dry isentropes. This difference is present in both hemispheres and throughout the entire year.

The discrepancy between the two circulations can be understood by looking at the joint distribution, $M(\theta_e, \theta)$, of the meridional mass transport at a given latitude ϕ. To obtain this distribution, we sorted the meridional mass flux $a\cos\phi v d\lambda \frac{\delta p}{g}$ by the value of θ and θ_e and integrated over time. Figure 2 shows the joint distribution obtained from the NCEP-NCAR Reanalysis at 40°N during December, January, and February, averaged between 1970 and 2004. By definition, the equivalent potential temperature is larger than the potential temperature, $\theta_e > \theta$, so the distribution is 0 below the diagonal $\theta_e = \theta$. In addition, the water content is roughly proportional to the difference $q \approx \frac{C_p}{L}(\theta_e - \theta)$, so that the further a parcel is above the diagonal, the higher its water content. The maximum amount of water vapor in an air parcel rapidly decreases with temperature due to the Clausius-Clapeyron relationship. The mass transport distribution becomes narrower in the upper-right corner of Fig. 2: This portion of the graph corresponds to upper tropospheric air parcels with low temperature and therefore low water vapor. The stream function at a given latitude Ψ_θ and Ψ_{θ_e} can be obtained by integrating the joint distribution $M(\theta_e, \theta)$ over selected portions of the domain. The mass transport between two dry isentropes θ_1 and θ_2 is given by the integral

$$\Delta\Psi_\theta = \Psi_\theta(\theta_2, \phi) - \Psi_\theta(\theta_1, \phi) = \int_{\theta_1}^{\theta_2}\int_0^{\infty} M(\theta_e, \theta) d\theta_e d\theta \quad (5)$$

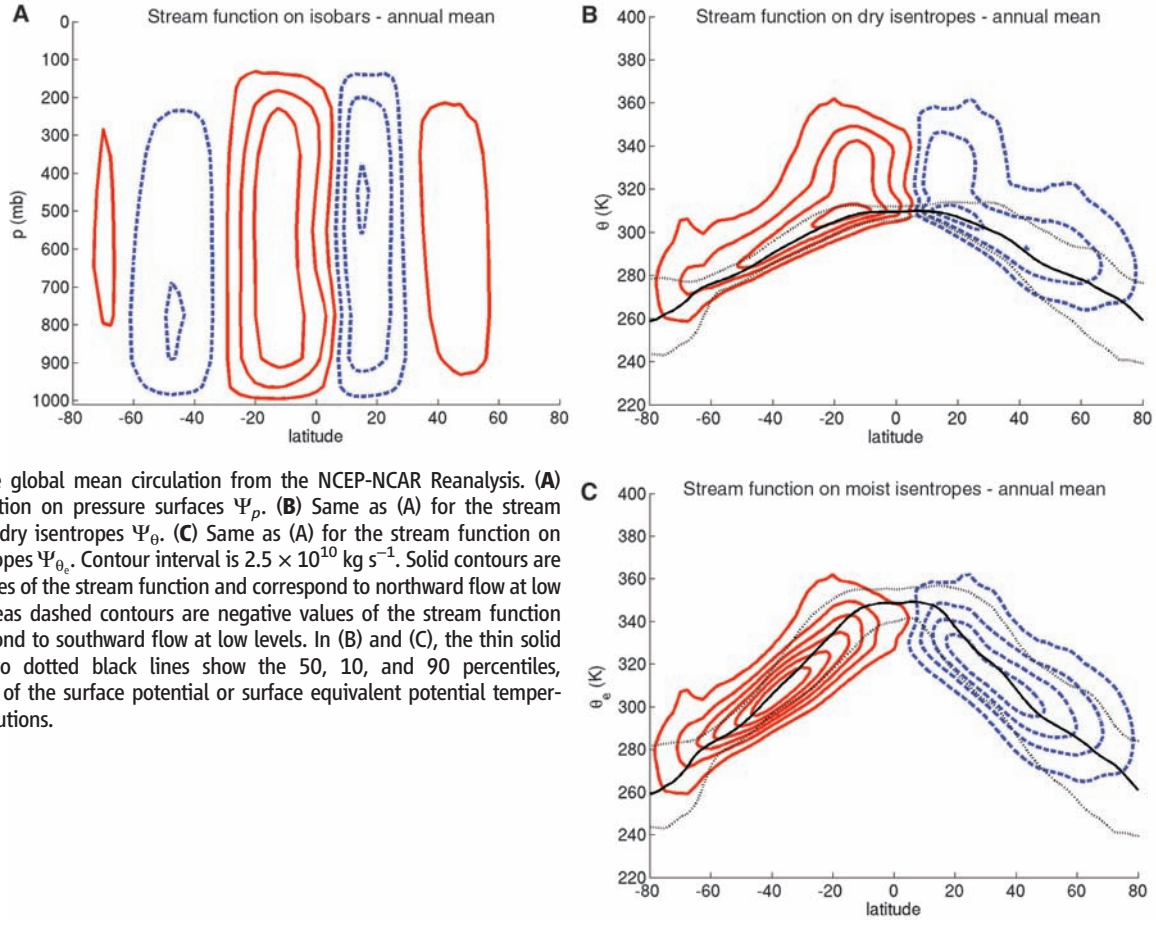

Fig. 1. The global mean circulation from the NCEP-NCAR Reanalysis. (**A**) Stream function on pressure surfaces Ψ_p. (**B**) Same as (A) for the stream function on dry isentropes Ψ_θ. (**C**) Same as (A) for the stream function on moist isentropes Ψ_{θ_e}. Contour interval is 2.5×10^{10} kg s^{-1}. Solid contours are positive values of the stream function and correspond to northward flow at low levels, whereas dashed contours are negative values of the stream function and correspond to southward flow at low levels. In (B) and (C), the thin solid line and two dotted black lines show the 50, 10, and 90 percentiles, respectively, of the surface potential or surface equivalent potential temperature distributions.

Similarly, the mass transport between two moist isentropes θ_{e1} and θ_{e2} is given by the integral

$$\Delta\Psi_{\theta_e} = \Psi_{\theta_e}(\theta_{e2}, \phi) - \Psi_{\theta_e}(\theta_{e1}, \phi) = \int_{\theta_{e1}}^{\theta_{e2}} \int_0^{\infty} M(\theta_e, \theta) d\theta d\theta_e \quad (6)$$

The integral in Eq. 5 is taken between two vertical lines in Fig. 2, whereas the integral in Eq. 6 is taken between two horizontal lines. It is apparent from Fig. 2 that the flow on moist isentropes (corresponding to horizontal lines in the figure) tends to point uniformly either toward the pole (at high values of θ_e) or toward the equator (at low values of θ_e). In contrast, the flow on dry isentropes (corresponding vertical lines) has contributions in both the equatorward and poleward directions. There is thus less cancellation between equatorward and poleward components of the flow when the circulation is integrated on moist isentropes than on dry isentropes, and the mass transport (Eqs. 5 and 6) is larger on moist isentropes than on dry isentropes. Because the equivalent potential temperature better separates poleward and equatorward flows, averaging on moist isentropes includes a larger portion of eddy mass transport into the global circulation.

The difference between the mass transports on dry and moist isentropes can be attributed to the contribution from the upper left quadrant of the distribution shown in Fig. 2. This corresponds to poleward moving air parcels with high θ_e and low θ. The poleward mass transport from this upper left quadrant cancels out with the equatorward flow at low θ and low θ_e when computing the mass transport on dry isentropes but is added to the poleward flow at high θ_e and high θ when computing the circulation on moist isentropes. The low potential temperature of these parcels is typical of the lower troposphere. In Fig. 2, the black contour line shows the values of θ and θ_e found at Earth's surface: This additional mass transport on moist isentropes corresponds to a low-level poleward flow of warm moist air. Its high equivalent potential temperature is indicative of air parcels that are nearly convectively unstable.

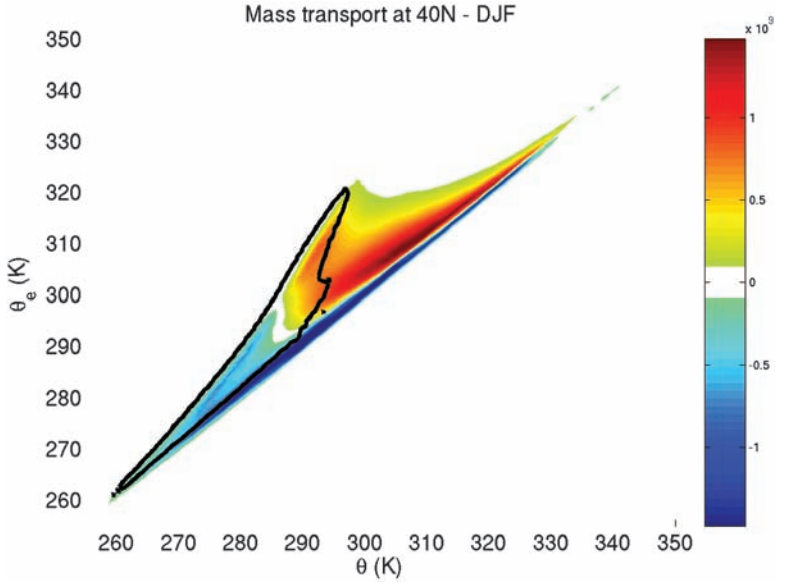

Fig. 2. Joint distribution of the mass transport as a function of θ and θ_e at 40°N during December, January, and February, averaged between 1970 and 2004. The combinations of (θ, θ_e) found within the black contour line have a high probability to be found at Earth's surface at 40°N, defined as having a probability density function larger than 0.001 K^{-2}.

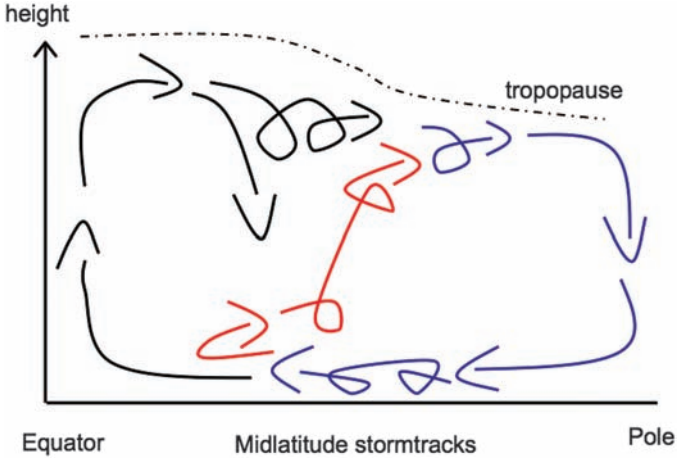

Fig. 3. Schematic representation of the global atmospheric circulation. Black and blue arrows indicate isentropic circulation on dry isentropes, with air rising at the equator, moving poleward in the upper troposphere, and returning equatorward near the surface. Red and blue arrows show the moist branch of the circulation corresponding to the additional mass transport on moist isentropes, with warm moist air moving toward the mid-latitudes at low levels, rising into the upper troposphere within the storm tracks, and subsiding over the pole and dry cold air moving toward the equator near the surface.

On the basis of these findings, we propose a revised description of the global atmospheric circulation in Fig. 3. It includes the previously identified global circulation on dry isentropes (black and blue arrows): Air rises to the upper troposphere within the precipitation zones of the equatorial regions and moves poleward; although some air subsides in the subtropics, the rest is advected poleward across the storm tracks by synoptic eddies, subsides over the poles, and returns equatorward near the surface (*4*, *5*). The additional mass transport found in the moist isentropes is associated with a "moist" branch of the circulation (red and blue arrows) in which low-level warm moist air in the subtropics is advected poleward by synoptic-scale eddies and rises within the storm tracks before subsiding over the poles and returning equatorward near Earth's surface. This moist branch is reminiscent of the Palmén-Newton circulation (*12*, *13*), which stresses the role of ascending warm air in mid-latitude eddies. These two branches of the circulation transport roughly the same amount of air: Half of the air parcels in the polar upper troposphere have risen within the storm tracks, whereas the other half rose within the equatorial regions.

This revised circulation emphasizes the importance of moist processes in mid-latitude dynamics. Although previous studies have noted some impacts of the moist processes on the isentropic circulation (*5*) and the transformed Eulerian mean circulation (*10*) in the mid-latitudes, we have shown that an analysis based on a dry framework systematically underestimates the atmospheric circulation by averaging out the moist branch of the circulation from the total mass transport. The moist branch is closely tied to the latent heat transport, which accounts for roughly half of the poleward energy transports (*2*). Ascent of warm, moist air within the storm tracks occurs through a combination of deep and slantwise convection (*14*, *15*) and results in enhanced precipitation. A key question is to what extent moist processes play an active role in setting the atmospheric lapse rate in mid-latitudes, as has been suggested recently (*16*, *17*). Without fully answering this question, our findings confirm that the circulation provides an ample supply of warm, moist air that should have a direct impact on the temperature structure in the mid-latitudes. As Earth's temperature rises, the amount of water vapor present in the atmosphere is extremely likely to increase as well (*18*). Understanding how changes in temperature and humidity affect the dynamics of the storm tracks and, in particular, the mass transport in the two branches of the cir-

culation is a critical issue for better predicting mid-latitude climate in a warmer world.

References and Notes

1. J. P. Peixoto, A. H. Oort, *Physics of Climate* (AIP Press, Melville, NY, 1992).
2. A. Czaja, J. Marshall, *J. Atmos. Sci.* **63**, 1498 (2006).
3. E. M. Kalnay *et al.*, *Bull. Am. Meteorol. Soc.* **75**, 437 (1996).
4. I. M. Held, T. Schneider, *J. Atmos. Sci.* **56**, 1688 (1999).
5. R. D. Townsend, D. R. Johnson, *J. Atmos. Sci.* **42**, 1565 (1985).
6. D. R. Johnson, *Adv. Geophys.* **31**, 43 (1989).
7. G. Stokes, *Trans. Cambr. Philos. Soc.* **8**, 441 (1847).
8. D. G. Andrews, M. E. McIntyre, *J. Atmos. Sci.* **33**, 2031 (1976).
9. T. Dunkerton, *J. Atmos. Sci.* **35**, 2325 (1978).
10. H. J. Edmon, B. J. Hoskins, M. E. McIntyre, *J. Atmos. Sci.* **37**, 2600 (1980).
11. K. A. Emanuel, *Atmospheric Convection* (Oxford Univ. Press, Oxford, 1994).
12. E. Palmén, *Q. J. R. Meteorol. Soc.* **77**, 337 (1951).
13. E. Palmén, C. W. Newton, *Atmospheric Circulation Systems* (Academic Press, New York, 1969).
14. K. A. Emanuel, *Mon. Weather Rev.* **116**, 1805 (1988).
15. R. L. Korty, T. Schneider, *J. Clim.* **20**, 5977 (2007).
16. M. N. Juckes, *J. Atmos. Sci.* **57**, 3050 (2000).
17. D. M. W. Frierson, I. Held, P. Zurita-Gotor, *J. Atmos. Sci.* **63**, 2548 (2006).
18. I. Held, B. Soden, *J. Clim.* **19**, 5686 (2006).

19. This work was supported by NSF under grant no. ATM-0545047 and grant no. PHY05-51164.

25 April 2008; accepted 8 July 2008
10.1126/science.1159649

Targeting QseC Signaling and Virulence for Antibiotic Development

David A. Rasko,[1]* Cristiano G. Moreira,[1] De Run Li,[2] Nicola C. Reading,[1] Jennifer M. Ritchie,[3] Matthew K. Waldor,[3] Noelle Williams,[2] Ron Taussig,[4] Shuguang Wei,[2] Michael Roth,[2] David T. Hughes,[1] Jason F. Huntley,[1] Maggy W. Fina,[4] John R. Falck,[2,4] Vanessa Sperandio[1,2]†

Many bacterial pathogens rely on a conserved membrane histidine sensor kinase, QseC, to respond to host adrenergic signaling molecules and bacterial signals in order to promote the expression of virulence factors. Using a high-throughput screen, we identified a small molecule, LED209, that inhibits the binding of signals to QseC, preventing its autophosphorylation and consequently inhibiting QseC-mediated activation of virulence gene expression. LED209 is not toxic and does not inhibit pathogen growth; however, this compound markedly inhibits the virulence of several pathogens in vitro and in vivo in animals. Inhibition of signaling offers a strategy for the development of broad-spectrum antimicrobial drugs.

A key challenge for medicine is to develop new drugs against pathogens that are resistant to current antimicrobial agents (*1*, *2*). A promising strategy is to identify agents that inhibit microbial virulence without inhibiting growth, because these present less selective pressure for the generation of resistance (*3*–*5*). Many bacterial pathogens recognize the host environment by sensing and responding to the host adrenergic signaling molecules epinephrine and norepinephrine (NE) in order to promote the expression of virulence factors (*6*, *7*). These pathogens appear to use the same membrane-embedded sensor histidine kinase, QseC (*7*), to recognize both host-derived adrenergic signals and the bacterial aromatic signal autoinducer-3 (AI-3) to activate their virulence genes (*5*, *6*). Upon sensing any of these signaling molecules, QseC autophosphorylates and subsequently phosphorylates a transcription factor, QseB (Fig. 1A) (*7*), which initiates a relay to a complex regulatory cascade and leads to the transcription of key virulence genes (Fig. 1B) (*5*–*8*).

QseC homologs are present in at least 25 important human and plant pathogens (table S1), and *qseC* mutants of enterohemorrhagic *Escherichia coli* (EHEC) (Fig. 1C and fig. S1) (*7*), *Salmonella typhimurium* (Fig. 2A) (*8*), and *Francisella tularensis* (*9*) are attenuated in infected animals. Because of the central role of the AI-3/epinephrine/NE QseC receptor in promoting the virulence of several important pathogens, we tested the effectiveness of inhibitors of this receptor as broad-spectrum antimicrobial agents.

A library of 150,000 small organic molecules from the University of Texas (UT) Southwestern was screened at a 5 μM concentration in a high-throughput assay to identify inhibitors of QseC-dependent virulence gene activation in EHEC (fig. S2) (*10*). The first round of positive hits, which represented a diverse range of molecular architecture, was subjected to additional rounds of screening followed by preliminary evaluations for toxicity against bacterial cells in vitro. This yielded a pool of 75 potential inhibitors with median inhibitory concentration (IC_{50}) values at or below 10^{-5} M. One compound was selected based on its potency as compared with other lead molecules, minimal toxicity toward bacterial and human cell lines, and potential for chemical modification. This molecule was subjected to structure-activity studies to identify ways to improve its potency. The result, LED209 [*N*-phenyl-4-{[(phenylamino) thioxomethyl]amino}-benzenesulfonamide] (Fig. 1D), was prepared in three steps (fig. S3).

New types of antimicrobial agents are needed to treat EHEC infections because treatments based on conventional antibiotics have been associated with worse clinical outcomes (*11*), probably because antibiotics induce an SOS response that enhances EHEC virulence (*12*). The genes encoding Shiga toxin are located within the late genes of a λ bacteriophage (a bacteriaphage that infects bacteria) and are transcribed when the phage enters its lytic cycle upon induction of an SOS response in EHEC (*13*). Shiga toxins are responsible for the morbidity and mortality of these infections. Transcription of EHEC virulence genes is induced by AI-3 and epinephrine. Neither AI-3 nor epinephrine had any effect on promoting virulence in a *qseC* mutant (Fig. 1B).

It was reported (*7*) and we confirmed that purified QseC in a liposome binds to tritiated NE and that phentolamine (an alpha-adrenergic antagonist) antagonizes this binding to block QseC autophosphorylation. In contrast, propranolol (a β-adrenergic antagonist) has no effect on QseC (Fig. 1E). We found that NE binding can be directly antagonized by 5 pM, but not 5 fM, LED209. Autophosphorylation of QseC in response to 50 μM epinephrine is also inhibited in the presence of 5 pM LED209 (Fig. 1F).

Consequently, QseC-dependent virulence gene expression in response to epinephrine (Fig. 1G) and AI-3 (Fig. 1H) was inhibited in the presence of 5 pM LED209. LED209-mediated inhibition of virulence gene expression also inhibited the secretion of EspA and EspB, two proteins encoded within the locus of enterocyte effacement (LEE) that are required for EHEC to translocate bacterial proteins into host cells and cause attaching-effacing (AE) lesions (Fig. 1I). At 5 pM, LED209 abolished EHEC AE lesion formation on cultured epithelial cells (Fig. 1J). Unlike conventional antibiotics, LED209 does not kill or hinder EHEC growth (fig. S4) or trigger the EHEC SOS response. Consequently, it does not promote the expression of Shiga toxin; indeed, it decreases the expression of the *stxAB* genes that encode this toxin (Fig. 1H).

However, administration of LED209 to infant rabbits before, after, or along with EHEC resulted in only a modest (and statistically nonsignificant) reduction in EHEC colonization of the intestine (fig S5). The failure of LED209 to reduce EHEC colonization in this animal may be attributable to rapid absorption from the gastrointestinal (GI) tract (see below and fig. S6). A nonabsorbable formulation may be required for noninvasive human pathogens such as EHEC.

S. typhimurium encodes a homolog of the EHEC QseC (87% similarity) sensor kinase that also controls virulence gene expression (*14*) (Fig. 2C). EHEC and *S. typhimurium* QseC are functionally interchangeable (*14*), and a *S. typhimurium*

[1]Department of Microbiology, University of Texas (UT) Southwestern Medical Center, Dallas, TX 75390, USA. [2]Department of Biochemistry, University of Texas (UT) Southwestern Medical Center, Dallas, TX 75390, USA. [3]Channing Laboratory, Brigham and Women's Hospital, Harvard Medical School, Boston, MA 02115, USA. [4]Department of Pharmacology, University of Texas (UT) Southwestern Medical Center, Dallas, TX 75390, USA.

*Present address: Department of Microbiology and Immunology, University of Maryland School of Medicine, Baltimore, MD 21201, USA.

†To whom correspondence should be addressed. E-mail: vanessa.sperandio@utsouthwestern.edu